The vibrational spectrum of FeO_2^+ isomers—Theoretical benchmark and experiment

Toni M. Maier, A. Daniel Boese, Joachim Sauer, Torsten Wende, Matias Fagiani, and Knut R. Asmis

Citation: The Journal of Chemical Physics **140**, 204315 (2014); doi: 10.1063/1.4878667
View online: https://doi.org/10.1063/1.4878667
View Table of Contents: http://aip.scitation.org/toc/jcp/140/20
Published by the American Institute of Physics

The vibrational spectrum of FeO_2^+ isomers—Theoretical benchmark and experiment

Toni M. Maier,[1] A. Daniel Boese,[1] Joachim Sauer,[1,a)] Torsten Wende,[2,b)] Matias Fagiani,[2] and Knut R. Asmis[2,3,c)]

[1]*Institut für Chemie, Humboldt-Universität zu Berlin, Unter den Linden 6, D 10099 Berlin, Germany*
[2]*Fritz-Haber-Institut der Max-Planck-Gesellschaft, Faradayweg 4-6, D 14195 Berlin, Germany*
[3]*Wilhelm-Ostwald-Institut für Physikalische und Theoretische Chemie, Universität Leipzig, Linnéstrasse 2, D-04103 Leipzig, Germany*

(Received 12 March 2014; accepted 7 May 2014; published online 28 May 2014)

Infrared photodissociation is used to record the vibrational spectrum of $FeO_2^+(He)_{2-4}$ which shows three bands at 1035, 980, and 506 cm^{-1}. Quantum chemical multi-reference configuration interaction calculations (MRCISD) of structures and harmonic frequencies show that these bands are due to two different isomers, an inserted dioxo complex with Fe in the +V oxidation state and a side-on superoxo complex with Fe in the +II oxidation state. These two are separated by a substantial barrier, 53 kJ/mol, whereas the third isomer, an end-on complex between Fe^+ and an O_2 molecule, is easily converted into the side-on complex. For all three isomers, states of different spin multiplicity have been considered. Our best energies are computed at the MRCISD+Q level, including corrections for complete active space and basis set extension, core-valence correlation, relativistic effects, and zero-point vibrational energy. The average coupled pair functional (ACPF) yields very similar energies. Density functional theory (DFT) differs significantly from our best estimates for this system, with the TPSS functional yielding the best results. The other functionals tested are BP86, PBE, B3LYP, TPSSh, and B2PLYP. Complete active space second order perturbation theory (CASPT2) performs better than DFT, but less good than ACPF. © *2014 AIP Publishing LLC*. [http://dx.doi.org/10.1063/1.4878667]

I. INTRODUCTION

The interaction between iron and oxygen plays a major role in many chemical processes,[1] including biological processes such as the transport, the storage and the activation of molecular oxygen (O_2),[2,3] as well as industrial processes in which iron acts as catalyst for the epoxidation of organic compounds with molecular oxygen.[4] For example, iron is part of the active centers of cytochrome oxidases[3] and catechol dioxygenases,[5,6] in which it is responsible for the activation of O_2. In myoglobine[7] and hemoglobine,[8] it takes part in the storage and the transport of oxygen, respectively. Moreover, iron-containing compounds[9,10] and iron oxide surfaces[11] have the ability to activate C–H and C–C bonds, and they are also relevant for corrosion processes.[1] Hence, a fundamental knowledge of the principles of the oxygen activation on iron is essential for a deeper understanding of many catalytic reactions in which iron takes part.

Gas phase spectroscopy offers the possibility to study mass-selected iron oxide clusters in isolation,[9,10] i.e., in the absence of ligand and solvent effects. These clusters can show reactivity with respect to C–H bond activation as well.[9] The variety of model systems which have been investigated ranges from oxygen-poor[12] to oxygen-rich[13] clusters in three different charge states:[14] cationic,[15] neutral,[16] and anionic.[17] Iron oxide gas-phase clusters are accessible for a variety of spectroscopic methods. These include infrared photodissociation (IRPD),[18] Raman,[19] and UV–Vis[20] spectroscopy in combination with different isolation and separation techniques.

So far theoretical investigations mainly focused on structure determination using Kohn-Sham density functional theory (DFT).[21–24] For mononuclear species such as FeO^+, FeO_2^+, or FeO_2^- also more sophisticated *ab initio* methods, such as Coupled-cluster,[25] CASPT2,[26] and MRCI,[17] were applied. In the case of FeO_2^+[26] and FeO^+,[27] these calculations were done almost 20 years ago.

In the present work we report more accurate theoretical results on FeO_2^+ and provide a detailed comparison of the reliability and accuracy of different quantum mechanical methods, in particular multi-reference methods. We also examine the performance of DFT employing different functionals. Computed vibrational frequencies are compared with experimental data gained by IRPD measurements, which allows assigning the observed bands to geometric structures and electronic states.

II. INFRARED PHOTODISSOCIATION EXPERIMENTS

IRPD experiments are carried out on a previously described ion-trap tandem mass spectrometer,[28,29] which was temporarily installed at the "Free Electron Laser for Infrared eXperiments" (FELIX) user facility[30] in the FOM institute

a)Electronic mail: js@chemie.hu-berlin.de
b)Present address: Physical and Theoretical Chemistry Laboratory, Department of Chemistry, University of Oxford, South Parks Road, Oxford OX1 3QZ, United Kingdom.
c)Electronic mail: asmis@fhi-berlin.mpg.de

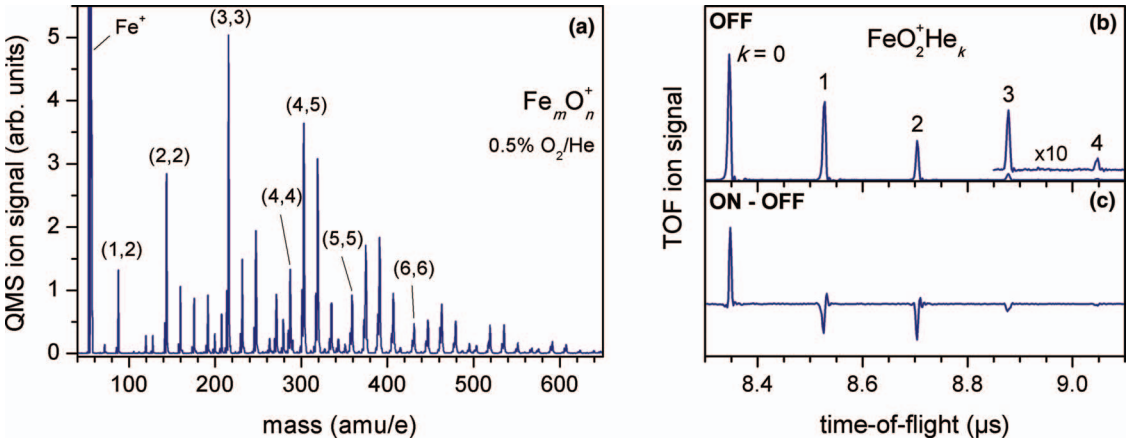

FIG. 1. (a) Typical mass spectrum of $Fe_mO_n^+$ clusters, labeled as (m,n), formed by laser vaporization. Source conditions are optimized to enhance the formation of FeO_2^+ cations. (b) TOF mass spectra of $FeO_2^+ \cdot He_k$ complexes ($k = 0$–4) recorded after irradiation with an IR laser pulse whose laser wavelength is tuned off resonance (14 μm) with any vibrational transition. The spectrum reflects the distribution of ion-He atom complexes formed inside the ion trap. (c) The bottom trace corresponds to the difference in ion yields when the laser wavelength is tuned on and off resonance with a vibrational transition around 9.7 μm. Ion depletion and formation is indicated by peaks pointing down and up, respectively.

Rijnhuizen (Nieuwegein, The Netherlands). A pulsed beam of cationic iron oxide clusters is formed by laser vaporization using a Smalley-type rotating rod source.[31] Vaporization is induced by focusing (30 cm focal length) the second harmonic output (532 nm) of a pulsed Nd:YAG laser (Quantel, BRIO) onto the surface of a moving iron-rod target. The formed plume is then entrained in a carrier gas pulse of 0.5% O_2 seeded in helium, and iron oxide clusters are subsequently formed through expansion in a clustering channel held at a temperature of 250 K. In order to obtain a stable cluster signal, the turning speed of the rod is set to ~3 turns per minute and laser pulse energies of up to 25 mJ are applied. Using a backing pressure of ~7 bars, oxygen-rich clusters are efficiently produced in the mass range from 100 to 600 amu, as displayed in Fig. 1(a) (left panel). The time delay between firing of the laser and opening of the pulsed valve is optimized to enhance the formation of FeO_2^+ clusters, labeled (1,2) in Fig. 1(a). The beam of ions passes a 4 mm diameter skimmer, is then collimated in a radio frequency (RF) buffer-gas-filled decapole ion-guide, and enters a quadrupole mass-filter that serves to mass-select FeO_2^+ ions. The mass-selected beam is focused into a cryogenically cooled RF ring electrode ion-trap. The trap is continuously filled with helium buffer gas at a trap temperature of 15 K, which allows for the accumulation and thermalization of the ions. Inside the ion trap, the bare FeO_2^+ ions undergo three-body collisions with the buffer gas, which promote the formation of weakly bound ion–He atom complexes.[32,33]

Under the present experimental conditions, FeO_2^+ is found to bind He atoms quite readily and a distribution of helium-tagged complexes $FeO_2^+ \cdot He_k$ is formed with $k = 1$–4 (Fig. 1(b), right panel); these complexes are used for the IRPD measurements. After loading the trap for 98 ms, all ions are extracted and focused both temporally and spatially into the center of the extraction region of an orthogonally mounted linear time-of-flight (TOF) mass spectrometer. Here, the ion packet is irradiated with a single FELIX Macropulse (~5 μs pulse width), and high voltage TOF extraction pulses are applied for recording a TOF mass spectrum. FELIX runs at a repetition rate of 10 Hz and is operated in the spectral region from 350 to 1200 cm^{-1}. The spectral bandwidth amounts to ~0.2% RMS of the central wavelength and pulse energies of up to 30 mJ are typically obtained. The IRPD spectra presented in Sec. IV D are spliced together from two scans, i.e., an overview scan (350–1200 cm^{-1}) measured using wavelength steps of 0.1 μm and a finer scan using 0.02 μm steps in the spectral region from 900 to 1200 cm^{-1} which covers the strongest absorption feature. The IRPD spectra are smoothed applying a 6-point (350–900 cm^{-1}) and a 26-point (900–1200 cm^{-1}) second-order polynomial Savitzky-Golay filter, respectively.

To obtain IRPD spectra 50–70 TOF mass spectra are summed for each wavelength step. The relative photodissociation cross section σ_{IRPD} is then determined from the relative abundances of the parent and photofragment ions, $I_P(\nu)$ and $I_F(\nu)$, and the frequency-dependent laser fluence $F(\nu)$ using $\sigma_{IRPD} \propto -\ln[I_P(\nu)/(I_F(\nu) + I_P(\nu))]/F(\nu)$. In more detail, all helium-tagged complexes $k = 1$–4 are considered as parent ions, and therefore $I_P(\nu)$ is defined as the sum of the corresponding TOF signals. Only the bare FeO_2^+ ion is considered as fragment ion. IR absorption manifests itself in the depletion of their corresponding TOF ion signal, accompanied with an increase of the bare FeO_2^+ ion signal (see Fig. 1(c)). In this manner, the extracted IRPD spectrum represents an average of the IR signatures of all helium-tagged complexes. In the analysis we additionally consider the most abundant complex $k = 1$ as fragment ion, and $k = 2$–4 as parent ions accordingly which allows to extract an averaged IRPD spectrum of the complexes $k = 2$–4. The comparison of both IRPD spectra provides spectroscopic information on how spectral features change as a function of the number of helium atoms attached.

Measuring IRPD spectra of $FeO_2^+ \cdot He_k$ complexes, in general, rather than of the bare FeO_2^+ ion is advantageous in several respects. First, the binding energy of FeO_2^+ is substantially larger than the photon energy. Hence, even if it were possible to deposit sufficient energy into the cluster via multiple photon absorption, the observed band positions and intensities would deviate substantially from the linear absorption

spectrum. Second, among the rare gas atoms, He exhibits the smallest polarizibility and consequently exerts the smallest perturbation on the structure of the bare ion. IRPD of the He-tagged complexes proceeds via loss of helium atoms which is reflected in changes of the corresponding TOF signals as mentioned above (Fig. 1(c)). Typically, He-tagging allows measuring action spectra close to the linear absorption regime.[18] Compared to dissociating the bare ion this ensures a more reliable comparison between IRPD spectra and simulated harmonic vibrational spectra, in order to assign structures.

III. COMPUTATIONAL METHODS

DFT calculations were performed with the TURBOMOLE 6.2 program suite.[34] We employed six different exchange-correlation functionals, the Generalized Gradient Approximation (GGA) functionals PBE[35] and BP86,[36] the meta-GGA TPSS,[37] the hybrid functionals B3LYP[38] and TPSSh[39] and the double hybrid functional B2PLYP.[40] Most of these calculations were done with Ahlrichs' TZVPP [5*s*, 3*p*, 2*d*, 1*f*] basis set,[41] named "def2–TZVPP" in the Turbomole library. In addition, also Ahlrichs' QZVPP ([7*s*, 4*p*, 3*d*, 2*f*, 1*g*]) basis set,[41] named "def2–QZVPP" in the Turbomole library and Grimme's dispersion correction (+D)[40] were used in some calculations to investigate basis set effects beyond the triple-ζ basis set and long range dispersion, respectively.

Multi-reference calculations were performed with the MOLPRO 2010 program package.[42] We chose complete active spaces (CAS) which contain the seven 4*s* and 3*d* electrons of the Fe ion and the eight 2*p* electrons of the O atoms (15 electrons, cf. Ref. 21). This CAS should be capable of describing the highest investigated octet spin state as well as the lower ones. The smallest possible active space is defined by 11 orbitals. For C_s-symmetry, seven active orbitals belong to the irreducible representation A′ and four active orbitals to A". Hence, we describe this complete active space as (7,4)-CAS. Similarly, we defined a (7,5)–CAS, a (8,4)–CAS, and a (8,5)–CAS. These active spaces were used for CASSCF calculations as well as the post-CASSCF methods CASPT2,[43] MRCISD and ACPF. We utilized Ahlrichs' TZVP ([5*s*, 3*p*, 2*d*, 1*f*]) and QZVP ([7*s*, 4*p*, 3*d*, 2*f*, 1*g*]) basis set,[41] as well as the aug'–cc–pwCVTZ ([6*s*, 5*p*, 3*d*, 1*f*] and [7*s*, 6*p*, 4*d*, 2*f*]) basis set[44] (the prime indicates augmentation only on O atoms). Davidson corrections (+Q)[45] were calculated using the relaxed coefficients of the reference configurations.

In addition, also two different sets of electrons, which are correlated in the post-CASSCF calculations, are chosen:

- A valence correlation space which consists of the 4*s* and 3*d* electrons of the iron and the 2*s* and 2*p* electrons of the O atoms.
- An augmented core + valence correlation space, which includes, in addition to the valence electrons, the 3*s* and 3*p* electrons of the iron and the 1*s* electrons of the O atoms.

For both multi-reference methods and DFT, scalar relativistic corrections were determined.[46] For this purpose, mass-velocity and Darwin correction terms were computed on the basis of the corresponding non-relativistic wave function.

The harmonic vibrational analysis for DFT was done with the standard module of TURBOMOLE (analytical second derivatives), while the CASPT2 and MRCISD harmonic frequencies were evaluated by numerical differentiation of energies. Differently from the standard module of MOLPRO, we used internal coordinates which for FeO_2^+ reduce the number of finite distortions for numerical hessian evaluation by a factor of up to seven.

IV. RESULTS AND DISCUSSION

A. Relative stabilities of different FeO_2^+ states

The general structural motifs of FeO_2^+ (Fig. 2), which were already mentioned by Schröder *et al.*,[21] are an inserted complex (Ia)–(Id), a side-on complex (IIa), and an end-on complex (IIIa) and (IIIb). Formally, these structures are associated with dioxide, peroxide and superoxide species, respectively. As we will discuss later, side–on complexes constitute superoxides and end-on structures are complexes of Fe^+ with an O_2 molecule. Inserted complexes can refer to dioxides with different oxidation states (Ia)–(Ic), ranging from +V to +III. Besides they can also correspond to a FeO^+ with an adsorbed oxygen radical (Id). Therefore, we distinguish the different species by their structural motif and not by their oxidation state.

To avoid geometrical restrictions, we performed all our calculations in C_s symmetry and distinguish A′ and A″ states. FeO_2^+ is an open-shell system and we investigated all spin states between $S = {}^1/_2$ (doublet) and $S = {}^7/_2$ (octet). The octet is related to the complex between triplet O_2 and high-spin Fe^+ ($3d^5\ 4s^2$) and is the highest reasonable spin state.

Structure optimizations for all states and structure types of the FeO_2^+ were performed with CASSCF, CASPT2, MRCISD, and ACPF using the TZVP basis set and the (7,4)-CAS. Table I shows the energies of the optimized structures for

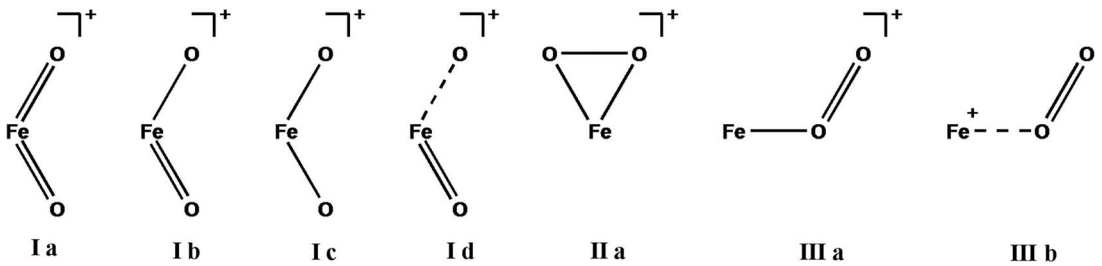

FIG. 2. The basic structures of FeO_2^+: different inserted complexes (Ia)–(Id), a side-on complex (IIa), and end-on complexes (IIIa) and (IIIb).

TABLE I. Relative energies (kJ/mol) of different states of FeO_2^+ determined with CASSCF, CASPT2, MRCISD(+Q), and ACPF with the TZVP basis set and the (7,4)-CAS. Values are calculated on minimum structures (see Tables F–L in the supplementary material[47]), except MRCISD+Q results, which are determined for MRCISD structures.

Structure	State	CASSCF	CASPT2	MRCISD(+Q)	ACPF
Side-on	$^6A'$	0	0	0 (0)	0
	$^6A''$	15	22	14 (17)	16
	$^4A'$	13	37	29 (31)	31
	$^4A''$	24	23	16 (19)	18
	$^2A'$	...[a]	28	76 (78)	79
	$^2A''$	...[a]	36	82 (81)	76
End-on	$^8A'$	35	214	184 (222)	226
	$^8A''$	30	186	188 (234)	238
	$^6A'$	34	69	60 (78)	80
	$^6A''$	32	71	61 (79)	81
	$^4A'$	33	62	56 (73)	75
	$^4A''$	30	64	57 (75)	76
	$^2A'$	32	49	52 (68)	70
	$^2A''$	29	48	53 (69)	68
Inserted	$^8A'$	161	...[a]	...[a]	...[a]
	$^8A''$	161	176	190 (191)	179
	$^6A'$	157	23	91 (72)	63
	$^6A''$	159	122	184 (166)	154
	$^4A'$	126	10	61 (46)	42
	$^4A''$	139	15	67 (46)	35
	$^2A'$	106	22	51 (42)	41
	$^2A''$	105	21	50 (40)	39

[a]No stable structures could be found.

different states. For MRCISD, the Davidson corrected energies (+Q) are given in parentheses. The relative stabilities of six states of FeO_2^+ are given in Fig. 3. For every structure, we show the two most stable spin states. With MRCISD(+Q) as reference, CASPT2 is a major improvement compared to CASSCF for the end-on structures. For the end-on structures CASPT2 "overshoots" leading to deviations of the relative energies in opposite direction and still of the order of 15–20 kJ/mol. For the side-on complexes relative energies show little variation passing from CASSCF to CASPT2, but for the $^2A'$ and $^2A''$ states no stable structures could be found with CASSCF.

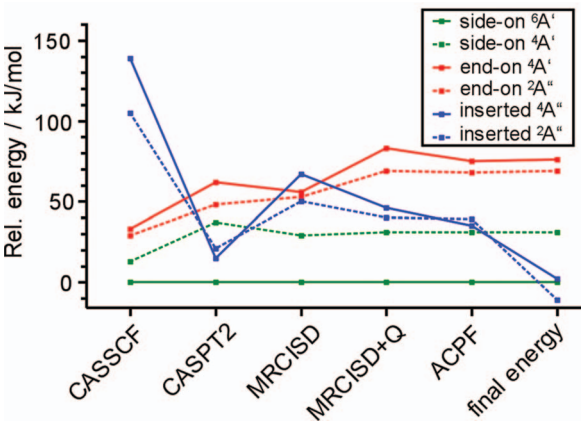

FIG. 3. Relative energies (kJ/mol) of six important states of FeO_2^+ determined with CASSCF, CASPT2, MRCISD, MRCISD+Q, and ACPF with (7,4)-CAS and TZVP basis set. The final energy (best estimate, discussed later) is also shown for comparison. For each structure the state with the lowest energy is shown.

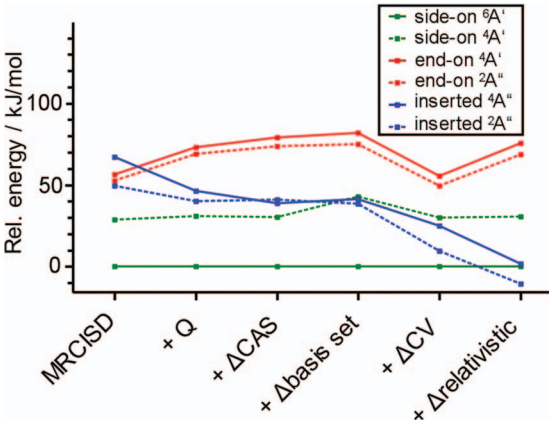

FIG. 4. Relative energies (kJ/mol) of the six states of Fig. 3 calculated with MRCISD/TZVP with stepwise addition of determined energy corrections (Q, ΔCAS, ΔCV, Δbasis set, and Δrelativistic).

The side-on complex in the $^6A'$ state is the global minimum for all methods. However, the relative stabilities of the low-spin states of the inserted complex strongly increase going from CASSCF to MRCISD (Fig. 4). This indicates that the side-on complex in the $^6A'$ state is a less correlated state and that the inclusion of additional correlation effects than it is the case using MRCISD could result even in a different lowest energy state. As we will show later, after adding further corrections the $^2A''$ state of the inserted complex will become the global minimum. Generally, the lower the spin, the less stable the side-on complexes are. In contrast, end-on and inserted complexes in states with lower spins are more stable, with the exception of the quartet states of the inserted complex using CASPT2.

The stabilities of the end-on and inserted complexes relative to the most stable side-on complex vary strongly across different methods. For CASSCF, the end-on complexes are destabilized by around 30 kJ/mol, and the inserted complexes by 105–161 kJ/mol. For CASPT2, the end-on complexes are 48–71 kJ/mol less stable, whereas the inserted complexes are only 10–23 kJ/mol higher in energy. MRCISD yields similar results to CASPT2 with the exception of the inserted complexes and the side-on complexes with $S = {}^1/_2$. For inserted complexes, values in between CASSCF and CASPT2 are obtained. Adding the Davidson correction stabilizes the inserted and destabilizes the end-on complexes by 10–20 kJ/mol. The resulting MRCISD+Q values are very close to those obtained by ACPF which also partially corrects size consistency errors. Hence, the Davidson correction is desirable for a more reliable description of the system.

Dynamic electron correlation effects strongly destabilize states with a spin of $S = {}^7/_2$. For the end–on structures, this state corresponds to a complex of molecular oxygen with high–spin Fe^+. The inserted complex in the $^8A''$ state corresponds to FeO^+ with an oxygen radical attached to it. However, the used complete active space is only minimal for calculations on the octet states and thus, size consistency problems are probably not fully corrected by MRCISD+Q and ACPF.

TABLE II. Relative energies (kJ/mol) of different states of FeO_2^+ using MRCISD with (7,4)–CAS and TZVP basis set. Energies are corrected with Davidson-correction[45] (+Q) and correction terms for the CAS size, the core–valence interaction (CV), basis set size, and scalar relativistic effects. Correction terms are determined on MRCISD+Q level.

Structure	State	MRCISD	Q	ΔCAS	ΔCV	Δ Basis set	Δ Relativistic	Final energy
Side-on	$^6A'$	0	0	0	0	0	0	0
	$^6A''$	14	3	0	–10	0	1	8
	$^4A'$	29	2	–1	–13	12	1	31
	$^4A''$	16	3	1	–14	33	1	39
	$^2A'$	76	2	–19	–53	–4	9	12
	$^2A''$	82	–1	–20	–36	10	11	46
End-on	$^8A'$	184	38	(–86)[a]	–104	28	–9	(50)[a]
	$^8A''$	188	45	(–174)[a]	–28	–23	–9	(0)[a]
	$^6A'$	61	17	5	–28	3	20	78
	$^6A''$	61	19	7	–25	4	20	86
	$^4A'$	56	17	6	–26	3	20	76
	$^4A''$	58	18	8	–26	4	20	82
	$^2A'$	52	16	6	–26	2	19	70
	$^2A''$	53	16	5	–25	1	19	69
Inserted	$^8A''$	190	1	–11	–20	13	–9	165
	$^6A'$	91	–19	–4	–15	2	–14	41
	$^6A''$	184	–18	–15	–11	7	–20	126
	$^4A'$	61	–15	0	–20	1	–19	8
	$^4A''$	67	–21	–8	–16	3	–24	2
	$^2A'$	51	–9	1	–24	–3	–19	–3
	$^2A''$	50	–9	1	–29	–2	–20	–11

[a]Active space not adequate.

The energies are most likely less accurate than those of other states.

Up to this point, structure optimizations were done with (7,4)-CAS/TZVP, evaluation of dynamic electron correlation for the valence region and without inclusion of relativistic effects. To examine the effects of extending the complete active space and the basis set as well as of including core-valence correlation and scalar relativistic effects, we performed single-point calculations on the (7,4)–CAS/TZVP structures. Assuming all effects to be additive, we compute final relative stabilities, arriving at our best estimates. As we shall see later, the energy corrections are small, making these assumptions plausible. Because of the above mentioned, limited reliabilities of the octet states, energy correction terms were only calculated for states with spin smaller than $^7/_2$. All corrections were calculated with MRCISD+Q, shown in Table II. Additional CASPT2 and MRCISD corrections, calculated without Davidson correction, can be found in the supplementary material.[47] The CAS corrections are evaluated as difference between a larger CAS and the (7,4)-CAS using the TZVP basis set.

For CASPT2, we were able to utilize the (8,5)-CAS. Unfortunately, MRCISD+Q calculations could not be completed for the (8,5)-CAS. Hence, we make use of the (7,5)- and (8,4)-CAS. Since MRCISD is variational, the active space yielding the lowest energy was used when determining the correction. Differences between both active spaces are fairly small for the majority of states (see Table O in the supplementary material).[47] Only the end–on complex in the octet states shows large correction terms, since the active spaces used are not capable of describing these nearly dissociated states. Concerning the other CAS corrections, mainly the energies for the end-on complexes are changed and destabilized by 5–8 kJ/mol. This indicates that the (7,4)-CAS is sufficient in most states. Only the side-on complexes with $S = {}^1/_2$ and the inserted complexes with higher spins show a significant stabilization, so that a larger active space plays a more important role.

For the evaluation of core-valence electron correlation, we used the (7,4)-CAS and the aug'–cc–pwCVTZ basis set. With respect to the global minimum structure, all other states are stabilized by at least 10 kJ/mol. The energies of the end-on complexes change by 25–28 kJ/mol, while the effect for inserted and side-on complexes exhibits a larger range (10–53 kJ/mol for side-on complexes and 11–29 kJ/mol for inserted complexes). In general, high-spin states are less affected by core-valence interaction. Hence, dynamic electron correlation of the 3*s* and 3*p* electrons of the iron atom and the 1*s* electrons of the O atoms plays an important role and cannot be neglected.

We tested the basis set extension effect using the (7,4)-CAS in combination with the QZVP basis set. For most states, corrections vary from −4 to +7 kJ/mol and can be regarded as non-systematic corrections due to the larger basis set. Only the energies of some side-on complexes with spins lower than $S = {}^7/_2$ are more affected. Hence, for these states the use of a quadruple-ζ basis set is desirable.

Relativistic corrections were calculated with different basis sets and correlation spaces. Since all of these values (see the supplementary material[47]) are rather close in energy, the corrections determined with the (7,4)–CAS and the QZVP basis set are shown. The inserted complexes are stabilized by

15–25 kJ/mol, while the end-on complexes are destabilized by around 20 kJ/mol. With the exception of the doublets, the energies of the side-on complexes are less affected. The size of the relativistic correction is similar to both Davidson and core-valence corrections, although no second row transition metal element is present.

Spin-orbit (SO) coupling effects are usually one order of a magnitude smaller, e.g., in $H_2Fe(CO)_4$,[48] and were disregarded. As further test, we performed SO-CI calculations (at the CASSCF level) on the lowest energy states of each structure (side-on $^6A'$, end-on $^2A''$, inserted $^2A''$) and on the $^8A'$ linear end-on complex which is expected to give the highest spin-orbit coupling effects. Following Ref. 49, our SO-CI calculations use five roots of the same spin for the examined states. The largest absolute lowering of the energy obtained for the three minimum states is 0.24 kJ/mol, whereas the energy of the octet of the linear end-on complex is lowered by 1.12 kJ/mol. We conclude that neglecting spin-orbit effects does not affect relative energies beyond an uncertainty of ±1 kJ/mol.

The summation of all energy correction terms leads to several changes in the ordering of the different states, see Fig. 4 for six important states of FeO_2^+. Relative to the side-on complexes, the inserted complexes are stabilized by 50–65 kJ/mol, whereas the end-on complexes are destabilized by 16–25 kJ/mol. The different behavior is due to the different signs of the Davidson correction and the relativistic corrections. As a result, the energies of the doublet and quartet states of the inserted complex become lower than and very similar to the energy of the $^6A'$ state of the side-on complex. We conclude that the inserted and the side-on complexes have minimum energy structures close in energy.

The uncertainty of our estimates is difficult to judge. Table I shows differences of up to 12 kJ/mol between MRCISD(+Q) and ACPF results. Similarly, the two ways of extending the CAS yield differences in the MRCISD(+Q) energies of up to 12 kJ/mol for the majority of structures/states (Table O in the supplementary material), although substantially larger differences also occur. Neglect of spin-orbit effects is found to lead to errors of the order of 1 kJ/mol. The estimates of core-valence correlation and basis set extension are also connected with (unknown) uncertainties, so that our estimate of the typical uncertainty is ±10 kJ/mol.

B. Electronic structure and iron oxidation state

For insight into the electronic structure and for assigning an oxidation state to iron, we make use of CASSCF spin densities and bond distances and angles of the investigated states. The CASSCF spin densities determined on MRCISD structures of the inserted, end-on and side-on complexes are shown in Figs. 5–7, respectively, together with Fe–O and O–O bond distances. The complete set of structural parameters can be found in the supplementary material.[47] For later use and comparison, TPSS spin densities are also displayed.

The **inserted complexes** can either represent dioxides (Ia)–(Ic) or an oxide with an oxygen radical attached to it (Id). This depends on whether Fe–O bonds are double bonds,

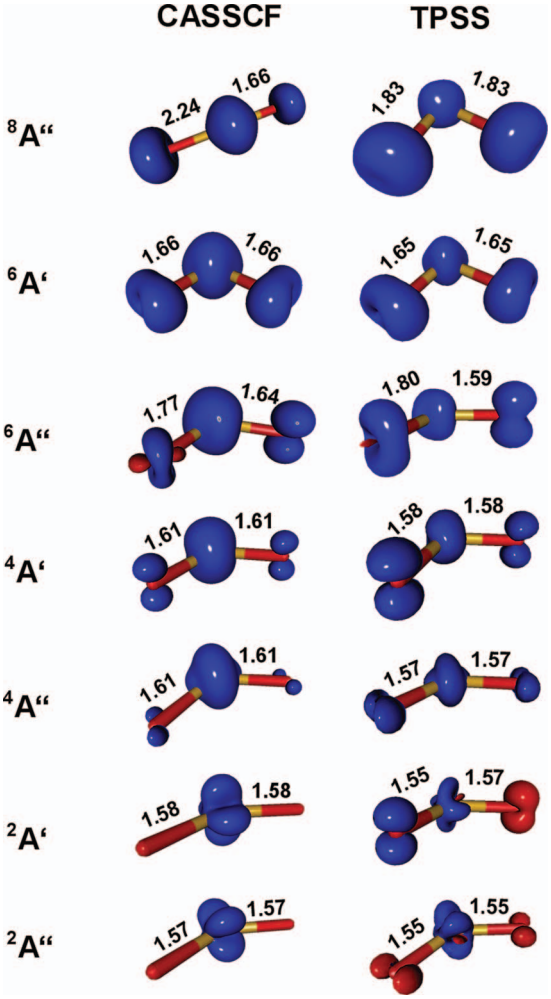

FIG. 5. Spin densities and Fe–O bond lengths (Å) of the inserted complexes, I, determined with CASSCF/TZVP and TPSS/TZVPP. CASSCF calculations were done on the MRCISD reference state and on MRCISD structures (Fe: yellow, O: red).

single bonds with an unpaired electron on the oxygen or oxygen radicals attached to an Fe-atom. While dioxides have C_{2v} symmetry, in oxides different Fe–O bond lengths lower the symmetry to C_s. Both doublet states (A' and A'') show spin density solely on the Fe atom, which corresponds to a dioxide with pure Fe=O double bonds and an iron atom oxidation number of +V (Ia). An Fe^{V+}=O active species with S = $^1/_2$ was already observed in a non–heme iron compound by Lyakin *et al.* using EPR.[50] The quartet states exhibit unpaired spin on both O atoms. Still being dioxides, the bond order is between one and two and the oxidation state of the Fe atom is in-between +III and +V. In the $^6A''$ state, the O atoms show partial biradical character, since the spin density on the O atoms is partially composed of an additional perpendicular p-orbital with the same spin as the main p-orbital. Hence, in this dioxide state the Fe atom has a formal oxidation number between +I and +III. Both, the $^6A''$ and the $^8A''$ state exhibit strong character of a monoxide, as indicated by the distortion from C_{2v} symmetry. In the $^6A''$ state there is an O atom in the singlet state strongly interacting with high-spin FeO^+. The longer Fe–O bond in the $^8A''$ state is evidence for

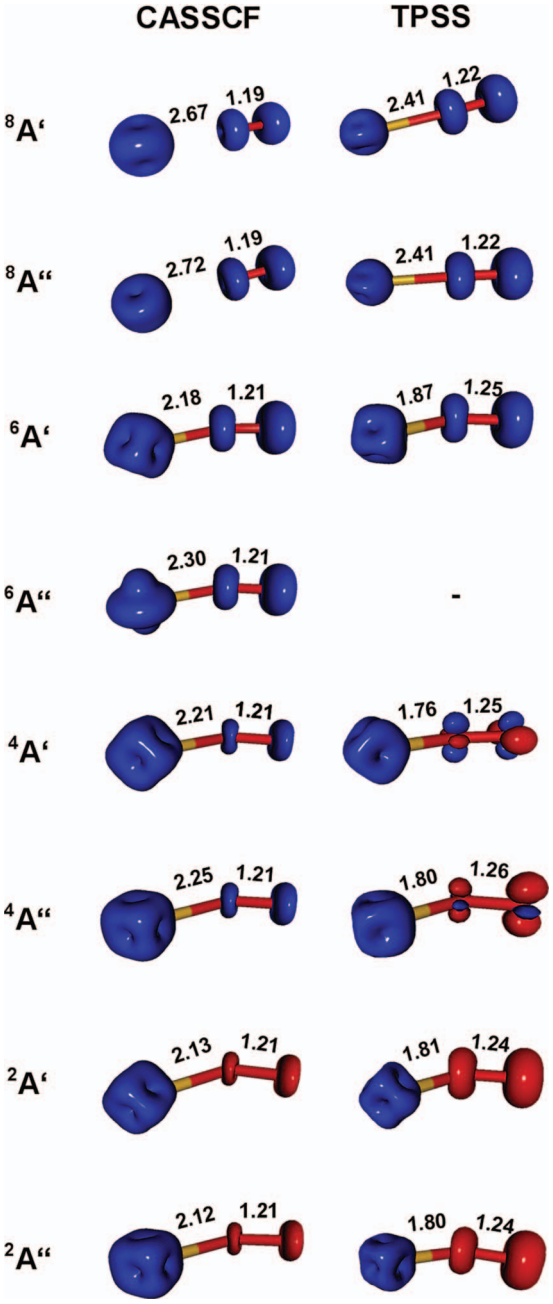

FIG. 6. Spin densities and bond lengths (Å) of the end-on complexes, III, determined with CASSCF/TZVP and TPSS/TZVPP. CASSCF calculations were done on the MRCISD reference state and on MRCISD structures (Fe: yellow, O: red).

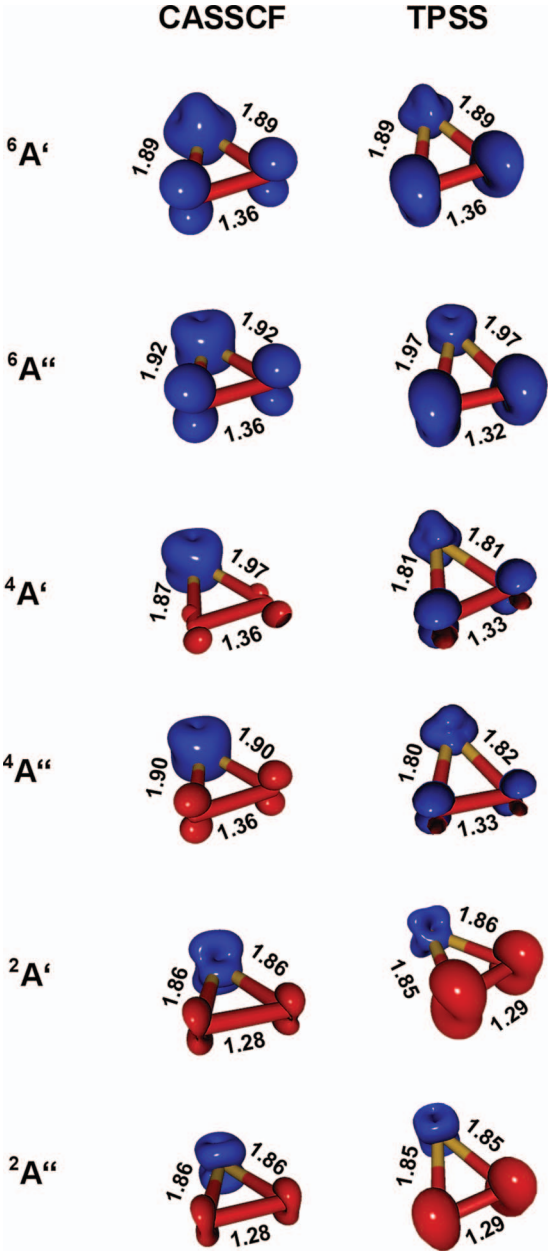

FIG. 7. Spin densities and bond lengths (Å) of the side-on complexes, II, determined with CASSCF/TZVP and TPSS/TZVPP. CASSCF calculations were done on the MRCISD reference state and on MRCISD structures (Fe: yellow, O: red).

a weaker interaction of the triplet O atom with the FeO^+ unit in this system.

Side-on and end-on complexes are Fe^+ ions with an O_2 species attached to it, that can constitute a peroxide, a superoxide or an oxygen molecule. The **end-on complexes III** in the different electronic states all contain molecular oxygen and the Fe oxidation number is +I. This follows from comparison of their O–O bond lengths shown in Fig. 6 with the ones of molecular oxygen and gas phase superoxide (MRCISD/TZVP), 1.19 and 1.32 Å, respectively. Formally, the doublet states can be composed of quartet (↑↑↑) or doublet Fe^+ (↑) and triplet O_2 (↓↓) or of doublet Fe^+ (↑) and singlet O_2 (↓↑). Similarly, the quartet states could consist of singlet (↓) or sextet Fe^+ (↑↑↑↑↑) with triplet O_2 (↓↓), or quartet Fe^+ (↑↑↑) with singlet O_2 (↓↑). The sextet states can be composed of quartet Fe^+ (↑↑↑) and triplet O_2 (↑↑) or of sextet Fe^+ (↑↑↑↑↑) and singlet O_2 (↓↑). In the octet states both Fe^+ and O_2 are in their high-spin state. Due to the multi-determinant ansatz of CASSCF, all mentioned configurations can contribute to one state. Nevertheless, since molecular oxygen is more stable in the triplet state, configurations with singlet O_2 should not contribute much, so that all states will mainly consist of molecular oxygen in the triplet state.

In contrast, in the **side-on complexes** the O_2 unit constitutes as superoxide, O_2^-, which implies an Fe oxidation number +II. The O–O bond lengths (Fig. 7) are closest to the one of gas phase superoxide (MRCISD/TZVP: 1.32 Å) and

TABLE III. Harmonic vibrational frequencies (cm^{-1}) of different states of FeO_2^+ determined by TPSS and B3LYP with TZVPP basis set in comparison to MRCISD and CASPT2 results (TZVP and (7,4)–CAS).

Structure	State	MRCISD	CASPT2	TPSS	B3LYP
Side-on	$^6A'$	1055/569/519	1021/555/551	1061/445/441	1166/455/402
	$^6A''$	1080/592/460	1050/ 590/474	1152/440/343	1209/437/352
	$^4A'$	1068/592/395	1034/589/429	1118/529/477	1092/488/350
	$^4A''$	1072/579/418	1050/578/422	1123/554/271	1194/474/316
	$^2A'$	1293/612/418	1318/487/336	1217/468/323	1358/332/309
	$^2A''$	1262/545/445	...	1218/458/330	1357/320/216
End-on	$^8A'$	...	...	1526/131/45	1622/114/64
	$^8A''$	...	...	1526/129/52	1622/115/60
	$^6A'$	1624/256/98	1592/253/99	1337/403/153	1476/324/121
	$^6A''$	1578/158/84	1561/170/95	...	...
	$^4A'$	1570/202/105	1535/228/121	1361/456/59	...
	$^4A''$	1569/182/103	1538/219/121	1276/472/113	...
	$^2A'$	1563/215/119	1451/239/119	1357/415/138	1541/292/143
	$^2A''$	1561/210/117	1446/251/126	1363/409/135	1529/308/150
Inserted	$^8A'$	...	...	642/586/165	697/609/152
	$^8A''$	...	...	680/272/253	667/319/143
	$^6A'$	851/639/240	830/624/231	892/624/269	911/535/273
	$^6A''$	887/739/333	...	910/649/204	884/680/204
	$^4A'$	925/835/300	869/791/309	948/939/359	974/951/359
	$^4A''$	902/831/245	889/782/243	997/953/306	1043/918/303
	$^2A'$	1005/863/219	934/794/252	1024/900/220	995/788/233
	$^2A''$	1011/872/215	948/805/105	1061/966/236	1070/681/224
ME[a] ΔMRCISD		0	–19	–10	–20
MAE[b] ΔMRCISD		0	34	97	89

[a]Mean error.
[b]Mean absolute error.

spin densities indicate only one unpaired electron in one of the π^* orbitals. Assuming spin down at O_2^- (↓), formally the doublet states of the side–on complexes could originate from singlet (↑↓) or triplet Fe^{2+} (↑↑), the quartet states from triplet (↓↓) or quintet Fe^{2+} (↑↑↑↑) and the sextet states from quintet (↓↓↓↓) or septet Fe^{2+} (↑↑↑↑↑↑).

For states of side-on and end-on complexes, the type of the leading configurations could be estimated utilizing the sign of the spin densities. For example, the $^4A''$ state of the side-on complexes shows different signs for the superoxide and the Fe^{2+}. Hence, the leading configuration should include quintet and not triplet Fe^{2+}. Nevertheless, configurations with triplet Fe^{2+} are not generally excluded. Similar considerations could be made on the other states, too.

C. Geometrical structure and harmonic frequencies

Vibrational frequencies are primarily given by geometrical structures. Bond lengths and angles of different isomers and states of FeO_2^+ using different methods can be found in the supplementary material.[47] As expected from the relative stabilities, ACPF and MRCISD yield similar results. Bond lengths deviate by a maximum of 2 pm, except for the Fe–O bond of the end-on complexes where they can differ by up to 10 pm. Angles vary up to 2°; only the $^6A''$ state of the inserted complexes shows larger deviations. Qualitatively, CASPT2 is able to reproduce ACPF/MRCISD structures, with bond lengths differing up to 31 pm and angles up to 12°. In contrast, structures obtained with pure CASSCF are very different.

Harmonic vibrational frequencies were calculated with CASPT2 and MRCISD in combination with the TZVP basis set and the (7,4)-CAS. Results are shown in Table III together with DFT results. Zero-point vibrational energies (ZPVE) have only a minor effect on the relative energies. For the side-on complexes, deviations between MRCISD and CASPT2 harmonic frequencies are relatively small, but deviations increase to 71 cm^{-1} for the inserted complexes and to up to 115 cm^{-1} for the end-on complexes. Because of numerical instabilities, we were unable to determine the frequencies of inserted $^6A''$ and the side-on $^2A''$ complexes using CASPT2.

In Table IV, we display all states (except the octet end-on complexes for which no adequate active spaces were affordable – see, Sec. IV A) sorted by their final relative energies including ZPVE with their corresponding harmonic frequencies calculated by MRCISD. Given the uncertainty estimate of ±10 kJ/mol, we cannot safely predict the precise energetic sequence of states. Six different states are within a range of 20 kJ/mol: The doublets and quartets of the inserted complex and the sextets of the side-on complex. Within a range of 50 kJ/mol, all other further investigated states of the inserted and side-on complexes follow, with the exception of the inserted complex in the $^6A''$ state. Generally, end-on complexes are much less stable than the other two isomers.

D. Structural assignment

Figure 8 (top panels) presents the averaged IRPD spectra of the helium-tagged complexes with $k = 1$–4 (panel (a)) and

TABLE IV. Final relative energies (kJ/mol) of different states of FeO_2^+ using MRCISD with (7,4)–CAS and TZVP basis set, applying all so far discussed corrections and adding ZPVE. Frequencies (cm^{-1}) of all modes (symmetric and antisymmetric Fe–O stretching, O–O stretching) are shown. Bending modes are listed as one of the three bond stretching modes.

			Frequencies		
Structure	State	Rel. energy + ZPVE	Fe–O (asym)	Fe–O (sym)	O–O
Inserted	$^2A''$	0	1011	872	215[a]
Inserted	$^2A'$	8	1005	863	219[a]
Side-on	$^6A'$	11	519[b]	569	1055[a]
Inserted	$^4A''$	11	902	831	245[a]
Side-on	$^6A''$	18	460[b]	592	1080[a]
Inserted	$^4A'$	18	925	835	300[a]
Side-on	$^2A'$	24	612[b]	418	1293[a]
Side-on	$^4A'$	41	395[b]	592	1068[a]
Side-on	$^2A''$	46	445[b]	545	1262[a]
inserted	$^6A'$	49	851	639	240[a]
Side-on	$^4A''$	50	418[b]	579	1072[a]
End-on	$^2A''$	78	117[b]	210	1561
End-on	$^2A'$	79	119[b]	215	1563
End-on	$^4A'$	85	105[b]	202	1570
End-on	$^6A'$	88	98[b]	256	1624
End-on	$^4A''$	91	103[b]	182	1569
End-on	$^6A''$	95	84[b]	158	1578
Inserted	$^6A''$	136	887	739	333[a]
Inserted	$^8A''$	175	…	…	…

[a]O–Fe–O bending mode.
[b]O–O · · · Fe bending mode.

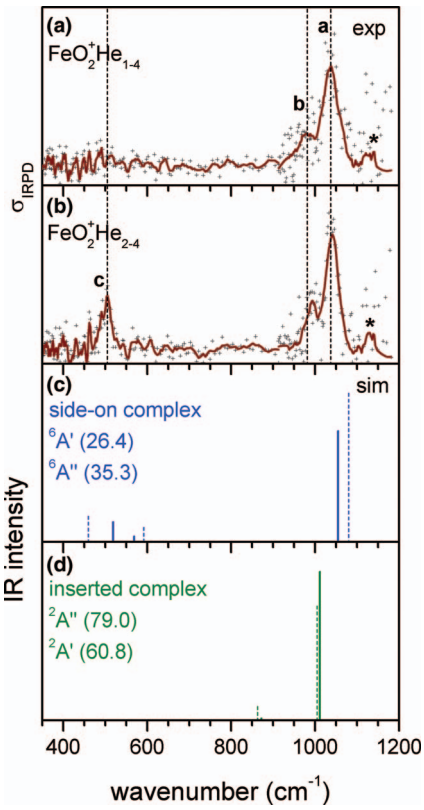

FIG. 8. Top: Experimental IRPD spectra of He-tagged complexes $FeO_2^+ \cdot He_{1-4}$ (a) and $FeO_2^+ \cdot He_{2-4}$ (b). The spectra are spliced from two scans and are smoothed applying a 6-point (350–900 cm^{-1}) and a 26-point (900–1200 cm^{-1}) second-order polynomial Savitzky-Golay filter. See text for labeling of the bands. Bottom: Calculated harmonic IR stick spectra of the energetically lowest two states of side-on ((c), blue, solid: $^6A''$ dash: $^6A'$) and inserted complexes ((d), green, solid: $^2A''$, dash: $^2A'$). The calculated absolute intensities (TPSS/TZVP) are given in parenthesis in km/mol.

k = 2–4 (panel (b) in the spectral region from 350 to 1200 cm^{-1}. These are compared to the calculated harmonic IR stick spectra (bottom panels) of the two most stable electronic states of the side-on ((c), blue) and inserted complexes ((d), green). We observe three absorption features, i.e., a broad, structured band in the higher wavenumber region centered around 1025 cm^{-1} emerging in both spectra (a) and (b), and a less intense band (labeled c) at 506 cm^{-1} which is only present in spectrum (b). The broad absorption band shows two characteristic absorption peaks (labeled a, b) whose positions depend on the number of He atoms present in the complex. In spectrum (a) peaks a (1037 cm^{-1}) and b (980 cm^{-1}) are separated by 57 cm^{-1}. In spectrum (b), which does not contain spectral contributions from the complex $k = 1$, both peaks a and b are blueshifted by +5 cm^{-1} and +12 cm^{-1}, respectively, thereby decreasing the peak separation to 50 cm^{-1}.

For the structural assignment we only consider the minimum energy states of the inserted and side-on complexes, as the end-on complexes are predicted more than 78 kJ/mol (Table IV) higher in energy, and, thus, are not expected to be formed under the present experimental conditions. Only the side-on complexes are predicted to exhibit IR-active vibrational modes in the 400–600 cm^{-1} region (see Table IV) and hence band c (506 cm^{-1}) can be unambiguously assigned to the antisymmetric Fe-O_2 stretching mode of such a side-on complex. The best agreement for band c is found for the lowest energy side-on complex $^6A'$ (519 cm^{-1}), while all other states exhibit antisymmetric stretching modes that are predicted at least 46 cm^{-1} higher or lower in energy. The side-on complexes exhibit two IR active modes. The O–O stretching mode of the $^6A'$ state is calculated at 1055 cm^{-1}, close to band a (1037 cm^{-1}) with substantial IR intensity and hence we assign it accordingly.

This leaves b (980 cm^{-1}) unassigned, which must originate from a different electronic state. Since all the electronic states corresponding to side-on complexes exhibit O–O stretching modes that are higher in energy compared to this mode in the $^6A'$ state it seems likely that band b can be attributed to the antisymmetric FeO_2 stretching mode of an inserted complex (panel (d)).

The most likely candidates are global minimum energy state $^2A''$ (1011 cm^{-1}) and the second lowest energy state $^2A'$ (1005 cm^{-1}), calculated +8 kJ/mol higher in energy. Their IR intensity is predicted to be roughly twice as large as the O–O stretch of the side-on complexes, while the intensity of band b is less than half of that of band a. Even if sextet states are three times more likely to occur than doublet states, this suggests that the inserted complexes as global minimum energy states of FeO_2^+ may be populated less than the side-on complexes in our experiment, presumably because the latter are easier to from under the present experimental conditions.

The inserted complexes exhibit two additional IR active modes, the symmetric FeO_2 stretch at ∼870 cm^{-1} and the FeO_2 bending mode at ∼215 cm^{-1}. The latter mode lies outside the detection window, while the first mode is predicted

TABLE V. Relative energies (kJ/mol) of different states of FeO_2^+ determined by different DFT functionals with TZVPP basis set in comparison to MRCISD results, Mean deviations (ME), and mean absolute deviations (MAE) are given.

Structure	State	BP86	PBE	TPSS	B3LYP	TPSSh	B2PLYP[a]	MRCISD[b]
Side-on	$^6A'$	0	0	0	0	0	0	0
	$^6A''$	19	19	12	5	6	4	7
	$^4A'$	8	7	9	60	34	64	30
	$^4A''$	14	12	16	18	45	95	39
	$^2A'$	26	26	17	44	30	44	3
	$^2A''$	33	33	27	52	41	59	35
End-on	$^8A'$	161	166	167	107	135	91	...[c]
	$^8A''$	161	166	167	107	135	91	...[c]
	$^6A'$	41	43	43	41	45	42	58
	$^6A''$	...[d]	...[d]	...[d]	...[d]	...[d]	4	66
	$^4A'$	44	44	45	...[d]	53	85	56
	$^4A''$	34	34	36	...[d]	...[d]	...[d]	62
	$^2A'$	51	52	46	45	49	46	50
	$^2A''$	49	50	46	44	50	47	50
Inserted	$^8A'$	204	211	198	208	205	221	...[d]
	$^8A''$	190	196	187	202	197	118	...[c]
	$^6A'$	11	14	17	100	66	221	55
	$^6A''$	122	126	125	187	162	233	147
	$^4A'$	–24	–24	–4	132	76	108	26
	$^4A''$	–17	–16	7	146	92	206	25
	$^2A'$	–31	–31	–13	129	71	213	16
	$^2A''$	–35	–35	–15	141	78	218	9
ME ΔMRCISD		–19	–18	–15	40	16	60	0
MAE ΔMRCISD		23	23	17	46	21	70	0

[a]Calculated on TPSS structure.
[b]Including Q, ΔCAS, ΔCV and ΔBasis set.
[c]No reliable values obtained.
[d]No stable structure found.

to be much less intense (see Fig. 8(d)) than the antisymmetric stretching mode and hence difficult to be observed at the current signal-to-noise level. The experimental spectra show an additional feature (marked with an asterisk) around 1125 cm^{-1} which we do not include in the present assignment. Its origin remains unclear. It may be an artefact of the applied smoothing filter, since the plotted cross section is particularly noisy in this range, due to the strongly decreasing laser pulse energies with increasing photon energy in this spectral region.

The absence of band c in spectrum (a) shows that the smallest complex, $FeO_2^+ \cdot He$ ($k = 1$), does not dissociate at ~500 cm^{-1}. This observation is in line with the estimated dissociation energy for this complex of about 1200 cm^{-1}. Owing to its relatively high dissociation energy the photodissociation process becomes less efficient at lower photon energies, i.e., the absorption of multiple photons is required to exceed the dissociation limit. In contrast, the presence of band c in spectrum (b) suggests that the dissociation energy of the larger complexes, $FeO_2^+ \cdot He_k$ with $k = 2$–4, is significantly lower.

E. Assessment of DFT

Large-scale MRCISD calculations will not be applicable to larger iron oxide gas-phase clusters. Thus, we performed DFT calculation on FeO_2^+ and compared them to our best MRCISD results. We used the GGA functionals PBE and BP86, the meta-GGA functional TPSS, the hybrid functionals B3LYP and TPSSh and the double hybrid functional B2PLYP. With the exception of B2PLYP, we did structure optimizations for all states with the TZVPP basis set. B2PLYP calculations used the TPSS structures.

Our reference MRCISD values are corrected for size consistency (Davidson correction), complete active space, basis set and core electron correlation. In Table V, we show the individual relative stabilities as well as the mean (ME) and the mean absolute deviation (MAE) from MRCISD results.

Despite several attempts, we were unable to locate the minimum structures for some end-on states using DFT. B2PLYP and both hybrid functionals correctly predict the $^6A'$ side-on complex as global minimum, whereas TPSS and the GGAs give lower energies for the inserted complexes. However, the hybrid functionals and B2PLYP strongly destabilize the inserted complexes, whereas the GGA functionals and TPSS show much smaller deviations for the inserted complexes. All low spin states of the side-on complex are destabilized by the hybrid functionals compared to the GGA functionals. Relative stabilities of the end-on complexes are similar for all functionals. The mean absolute deviation of TPSS is the lowest, followed by TPSSh and the GGAs. The use of B3LYP and B2PLYP can be discouraged.

Concerning the structures shown in the supplementary material,[47] TPSS, PBE, and BP86 yield very similar results, whereas B3LYP and TPSSh differ. The deviations are as large

as 13 pm in bond lengths and 20° in angles using different functionals. Compared to MRCISD, the Fe–O bonds of the end-on and inserted complexes are generally too short. For side-on complexes, the GGAs systematically exhibit too short Fe-O bonds. For the end-on complexes, all O−O bond lengths are overestimated. Bond angles are in good agreement with the MRCISD structures with the exception of the Fe-O_2 angle in the end-on complexes: MRCISD shows angles between 132° and 151°, while the angles of the quartet states calculated with DFT are almost linear, with the exception of TPSS.

Harmonic frequencies calculated with TPSS and B3LYP are compared with CASPT2 and MRCISD frequencies in Table III. For most states, both functionals give deviations of up to 100 cm^{-1} from MRCISD.

For the end-on complexes, TPSS frequencies of the O−O stretching mode are underestimated by a large amount, with B3LYP yielding too large frequencies for the sextet states of the side-on complex. Remember that these are the two minimum energy states for the MRCISD reference. Although the less stable end-on complexes are not well described with TPSS, it produces the qualitative picture of the harmonic MRCISD frequencies.

Concerning relative stabilities, geometrical structures and harmonic frequencies, TPSS yields the best results. Although it is not accurate enough for quantitative calculations, it is suited for qualitative discussions. Here, all important states are within a range of 50 kJ/mol. We were able to reproduce most MRCISD structures with TPSS, while harmonic frequency evaluation is only qualitatively possible. This conclusion is in agreement with previous DFT results on small transition metal compounds of Furche *et al.*[51]

Finally, in Figs. 5–7 we compare TPSS spin densities of all states with CASSCF results calculated at MRCISD structures. The spin densities of the end-on and side-on complexes are overall in good agreement with CASSCF. Only the quartet states show molecular oxygen in a singlet state. For the inserted complexes the sextets and quartets are qualitatively well described, while TPSS converges into a different state for the $^8A''$ irreducible representation. In contrast to CASSCF, the doublet states exhibit spin density on the O atoms. The qualitative deviations from CASSCF spin densities can be ascribed to spin contamination, which is unavoidable in one-determinantal Kohn-Sham theory. As a result, DFT describes different states with different quality, which also affects the relative stabilities.

F. Isomerization of FeO_2^+ structures

To answer the question if isomerization of different structures could affect the experimental IRPD spectrum, we examined the potential energy surfaces for interconversion of the different isomers. We consider only the transitions between the inserted and the side-on complexes, and between the side-on and end-on complexes. For three different spin states (doublet, quartet, sextet) transition structure optimizations were performed using TPSS/TZVPP (see the supplementary material)[47] and the Turbomole code.[34] Between the minimum and the transition structures, we calculated a potential energy curve by linear interpolation of the coordinates. Figure 9 shows the relative energies along this path. Due to the high computational cost of transition structure optimizations we were unable to perform MRCISD calculations. The use of MRCISD single point energies calculated at TPSS structures is also not recommended because of the large deviations of DFT structures, even for energy minima.

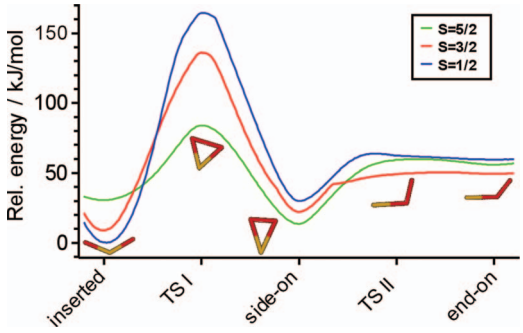

FIG. 9. Transitions between different structures of FeO_2^+ for doublet, quartet, and sextet states calculated with TPSS/TZVPP. Relative energies are given in kJ/mol, structure diagrams: orange – Fe, red – O.

We obtain a significant barrier between the inserted and the side-on complexes. Compared to the results of Schroeder *et al.*,[21] the energy barrier between the side-on and inserted complex is much higher, around 50 kJ/mol for the sextet and around 160 kJ/mol for the doublet state. All transitions between the inserted and the side-on structures should be very slow. In contrast, the energy barrier between the side-on and end-on complexes is very low and the latter can be regarded as a precursor of the side–on complexes.

If both, the inserted and the side-on structures are generated during the experiment, but the high barrier will prevent isomerization of the side-on into the more stable inserted complexes. This could explain that band b assigned to the inserted complex (Fig. 8) is less intense than band a assigned to the side-on complex.

V. CONCLUSIONS

Comparing different multi-reference methods for FeO_2^+, we found that MRCISD performs best in both structure optimizations and harmonic frequency calculations. Core electron correlation, relativistic effects and size consistency corrections of MRCISD are all found to contribute significantly to the relative stabilities of the isomers, whereas extension of the complete active space and the basis set provide minor changes only.

The calculations for different isomers (inserted, side-on, end-on) and different spin states show that the observed double band of the IRPD spectrum is due to two species, an inserted and a side-on complex. Both species may be present in an experiment because a high barrier prevents interconversion of the less stable side-on (superoxo) in the more stable inserted (dioxo) complex.

Concerning the electronic structure, end-on complexes are ion-molecule complexes of Fe^+ with O_2, whereas the side-on complexes are superoxides with Fe in the oxidation state

+II. Inserted complexes are dioxides with different oxidation numbers on the Fe atom or monoxides with an attached O atom. The most stable inserted complex ($^2A''$) is a dioxide with Fe^{+V} in a low spin configuration.

From the assessment of different density functionals based on the MRCISD data we learn that TPSS performs best.

ACKNOWLEDGMENTS

This work has been supported by German Research Foundation (DFG) within CRC 1109 and by the Funds of the Chemical Industry (FCI). We thank Professor Michael Dolg, Köln, for a useful hint.

[1]H. Wu, S. R. Desai, and L.-S. Wang, J. Am. Chem. Soc. **118**, 5296–5301 (1996).
[2]A. Natrajan, S. M. Hecht, G. A. van der Marel, and J. H. van Boom, J. Am. Chem. Soc. **112**, 3997–4002 (1990).
[3]B. T. Babcock and M. Wikström, Nature (London) **356**, 301–309 (1992).
[4]R. W. Saalfrank, S. Reihs, and M. Hug, Tetrahedron Lett. **34**, 6033–6036 (1993).
[5]L. Que, Jr., J. Chem. Educ. **62**, 938–943 (1985).
[6]H. G. Jang, D. D. Cox, and L. Que, Jr., J. Am. Chem. Soc. **113**, 9200–9204 (1991).
[7]H. Chen, M. Ikeda-Saito, and S. Shaik, J. Am. Chem. Soc. **130**, 14778–14790 (2008).
[8]M. F. Perutz, M. G. Rossmann, A. F. Cullis, H. Muirhead, G. Will, and A. C. T. North, Nature (London) **185**, 416–422 (1960).
[9]D. Schröder and H. Schwarz, Angew. Chem., Int. Ed. Engl. **32**, 1420–1422 (1993).
[10]S. Ye and F. Neese, Curr. Opin. Chem. Biol. **13**, 89–98 (2009).
[11]W. Weiss and W. Ranke, Prog. Surf. Sci. **70**, 1–151 (2002).
[12]G. L. Gutsev, S. N. Khanna, B. K. Rao, and P. Jena, J. Phys. Chem. A **103**, 5812–5822 (1999).
[13]H. Shiroishi, T. Oda, I. Hamada, and N. Fujima, Eur. Phys. J. D **24**, 85–88 (2003).
[14]D. Schröder, J. Phys. Chem. A **112**, 13215–13224 (2008).
[15]D. Schröder, P. Jackson, and H. Schwarz, Eur. J. Inorg. Chem. **2000**, 1171–1175 (2000).
[16]Z. Cao, M. Duran, and M. Solà, J. Chem. Soc., Faraday Trans. **94**, 2877–2881 (1998).
[17]Z. H. Li, Y. Gong, K. Fan, and M. Zhou, J. Phys. Chem. A **112**, 13641–13649 (2008).
[18]K. R. Asmis, Phys. Chem. Chem. Phys. **14**, 9270–9281 (2012).
[19]J. A. Crayston, M. J. Almond, A. J. Downs, M. Poliakoff, and J. J. Turner, Inorg. Chem. **23**, 3051–3056 (1984).
[20]D. N. Shin, Y. Matsuda, and E. R. Bernstein, J. Chem. Phys. **120**, 4157–4164 (2004).
[21]D. Schröder, A. Fiedler, J. Schwarz, and H. Schwarz, Inorg. Chem. **33**, 5094–5100 (1994).
[22]T. Vondrak, K. R. I. Woodcock, and J. M. C. Plane, Phys. Chem. Chem. Phys. **8**, 503–512 (2006).
[23]B.-F. Xu, C.-L. Yang, M.-S. Wang, and X.-G. Ma, Physica B **406**, 200–204 (2011).
[24]W. Xue, S. Yin, X.-L. Ding, S.-G. He, and M.-F. Ge, J. Phys. Chem. A **113**, 5302–5309 (2009).
[25]Z. Cao, M. Duran, and M. Solà, Chem. Phys. Lett. **274**, 411–421 (1997).
[26]D. Schröder, A. Fiedler, W. A. Herrmann, and H. Schwarz, Angew. Chem., Int. Ed. **34**, 2517–2520 (1995).
[27]A. Fiedler, J. Hrušák, W. Koch, and H. Schwarz, Chem. Phys. Lett. **211**, 242 (1993).
[28]D. J. Goebbert, G. Meijer, and K. R. Asmis, AIP Conf. Proc. **1104**, 22–29 (2009).
[29]D. J. Goebbert, T. Wende, R. Bergmann, G. Meijer, and K. R. Asmis, J. Phys. Chem. A **113**, 5874–5880 (2009).
[30]D. Oepts, A. F. G. van der Meer, and P. W. van Amersfoort, Infrared Phys. Technol. **36**, 297–308 (1995).
[31]T. Wende, "Gas phase infrared photodissociation spectroscopy of mass-selected ionic clusters: Metal oxides and microhydrated anions," Dissertation (Freie Universität Berlin, 2012).
[32]M. Brümmer, C. Kaposta, G. Santambrogio, and K. R. Asmis, J. Chem. Phys. **119**, 12700–12703 (2003).
[33]K. R. Asmis, T. Wende, M. Brümmer, O. Gause, G. Santambrogio, E. C. Stanca-Kaposta, J. Döbler, A. Niedziela, and J. Sauer, Phys. Chem. Chem. Phys. **14**, 9377–9388 (2012).
[34]TURBOMOLE V6.2 2010, a development of University of Karlsruhe and Forschungszentrum Karlsruhe GmbH, 1989-2007, TURBOMOLE GmbH, since 2007, see http://www.turbomole.com.
[35]J. P. Perdew, K. Burke, and M. Ernzerhof, Phys. Rev. Lett. **77**, 3865–3868 (1996).
[36]A. D. Becke, Phys. Rev. A **38**, 3098 (1988); J. P. Perdew, Phys. Rev. B **34**, 7406 (1986).
[37]J. Tao, J. P. Perdew, V. N. Staroverov, and G. E. Scuseria, Phys. Rev. Lett. **91**, 146401 (2003).
[38]A. D. Becke, J. Chem. Phys. **98**, 5648–5652 (1993).
[39]V. N. Staroverov, G. E. Scuseria, J. Tao, and J. P. Perdew, J. Chem. Phys. **119**, 12129 (2003); **121**, 11507 (2004).
[40]S. Grimme, J. Comput. Chem. **27**, 1787–1799 (2006).
[41]F. Weigend and R. Ahlrichs, Phys. Chem. Chem. Phys. **7**, 3297–3305 (2005).
[42]H.-J. Werner, P. J. Knowles, G. Knizia, F. R. Manby, M. Schütz *et al.*, MOLPRO, version 2010.1, a package of *ab initio* programs, 2010, see http://www.molpro.net.
[43]H.-J. Werner, Mol. Phys. **89**, 645–661 (1996).
[44]N. B. Balabanov and K. A. Peterson, J. Chem. Phys. **123**, 064107 (2005).
[45]E. R. Davidson and D. W. Silver, Chem. Phys. Lett. **52**, 403–406 (1977).
[46]R. D. Cowan and D. C. Griffin, J. Opt. Soc. Am. **66**, 1010–1014 (1976).
[47]See supplementary material at http://dx.doi.org/10.1063/1.4878667 for structure parameters and additional relative energies.
[48]V. Vallet, A. Strich, and C. Daniel, Chem. Phys. **311**, 13–18 (2005).
[49]X. Cao, Chem. Phys. **311**, 203–208 (2005).
[50]O. Y. Lyakin, I. Prat, K. P. Bryliakov, M. Costas, and E. P. Talsi, Catal. Commun. **29**, 105–108 (2012).
[51]F. Furche and J. P. Perdew, J. Chem. Phys. **124**, 044103 (2006).